

Supplementary Information

Water reduction by photoexcited silica and alumina

Raluca Musat^{1,2}, Georges Vigneron^{1,2}, David Garzella³, Sophie LeCaër^{2,1},
Jean-François Hergott³, Jean Philippe Renault^{1,2*}, Stanislas Pommeret^{1,2}

1 CEA, IRAMIS, Laboratoire de Radiolyse, 91191 Gif-sur-Yvette Cedex, France

2 CNRS, Laboratoire Claude Fréjacques, 91191 Gif-sur-Yvette Cedex, France

3 CEA, IRAMIS, SPAM, 91191 Gif-sur-Yvette Cedex, France

S.I. Materials

S.I.1 Controlled Pore Glasses

The *Controlled Pore Glasses* (CPG) have been intensely used since their discovery in the 1960s¹ due to their remarkable properties: high porosity and well-defined pore size, excellent mechanical properties and high thermal stability and resistance to acids. The pore size can be tuned during the fabrication process from 4 up to 300 nm as powders and up to 50 nm as thin plates.²

The CPGs are prepared from alkali borosilicate glasses by phase separation and combined acid and alkaline leaching treatments. As a result of the temperature-depending phase separation of alkali borosilicate glasses, two different phases are obtained: one of almost pure silica; and one being an alkali-rich borate phase with different amounts of silica dissolved in it. Because of the small solubility of silica in acids, it remains after the extraction as finely dispersed silica in the cavities of the main silica framework and affects the pore structure of microporous glasses. The treatment with alkaline solution removes the finely dispersed silica, and macroporous glasses are obtained. Ultrathin porous glass plates (0.2 x 1 x 1 cm) (figure S1) with pores between < 2 and 50 nm were supplied by CHEMIE PARC INSTITUT GmbH (Bitterfeld, Germany).

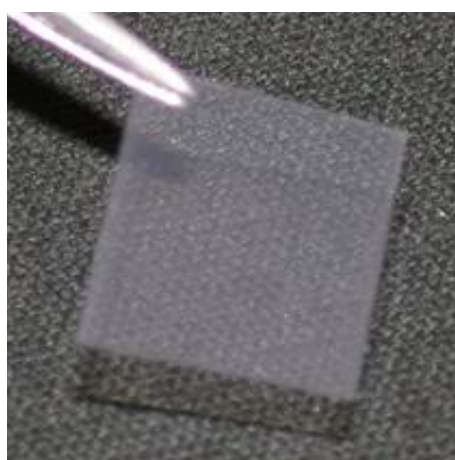


Figure S1: The optical transparency of the CPG sheets makes them a perfect system for pump-probe experiments.

The pore structure of the samples was characterised by nitrogen adsorption isotherms, in the case of the 1 nm pore sample (BJH method) and with the mercury intrusion technique in the case of the 13 and 50 nm pore samples. The main characteristics of the studied samples are presented in the table below:

Pore diameter (nm)	Wall thickness (nm)	Mean chord length (nm)	Specific surface (m ² /g)	Porosity (cm ³ /g)
1	4	0.9	330	0.12
50	50	12	39	0.42

Table S1: Spatial characteristics of the CPGs

S.I.2 Porous alumina

Alumina membranes (Anodisc aluminum oxide membrane filters, Whatman International) used in the present study are 13 mm wide and 60 µm thick, and have a porosity of ~50%. They contain 100 nm diameter parallel pores separated by 80 nm walls, arranged in a honeycomb-type morphology. These membranes are prepared by anodic dissolution of aluminium foils and have a typical specific surface of ~6 m²/g.

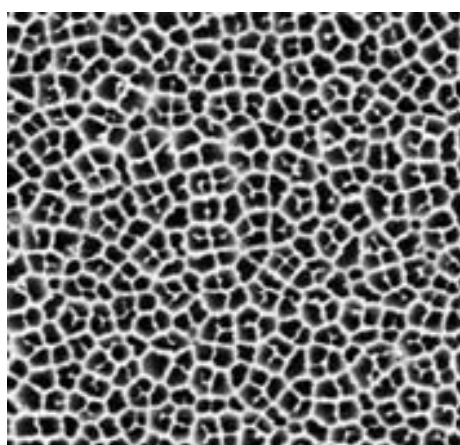


Figure S2: SEM picture of alumina nanoporous membranes.

S.II. Experimental set up

The transient absorption spectroscopy experiments were performed on PLFA (Plate-forme Lasers Femtosecondes Accordables), at DSM, CEA Saclay. The PLFA facility is based on a commercial kilohertz Titanium:Sapphire laser system (Amplitude Technologies PULSAR X-treme equipped with DPSS JADE lasers from THALES laser). The PLFA source delivered pulses centred around 800 nm, with a pulse energy of 12 mJ at 1 kHz repetition rate. The pump-probe set up is depicted in Figure S3. The output laser beam was passed through a half-wave plate and then reduced in diameter using a telescope. The laser frequency was doubled in a 0.2 mm thick BBO crystal (type I Beta-Barium-Borate crystal). The second harmonic (400 nm) beam was separated from the fundamental (800 nm) by dichroic mirrors and was directed onto a 0.1 mm thick BBO (type I) crystal in order to generate the third harmonic (266 nm) beam by sum-frequency mixing with the fundamental beam. The beam at 266 nm was separated from the 400 nm and 800 nm beams by dielectric mirrors and focused onto the sample. The energy of the 266 nm pump pulse could be varied from 10 µJ to 100 µJ using the half-wave plate on the 800 nm beam.

A continuous Helium:Neon laser beam (632.8 nm) was used as the probe beam. The probe signal was detected using a silicon photodiode (Thorlabs DET 210) and a digital oscilloscope (1.5 GHz bandwidth, Tektronix TDS 784D). The overall instrument response time is 2 ns as determined from the rise time of the transient absorption signal of the hydrated electron.

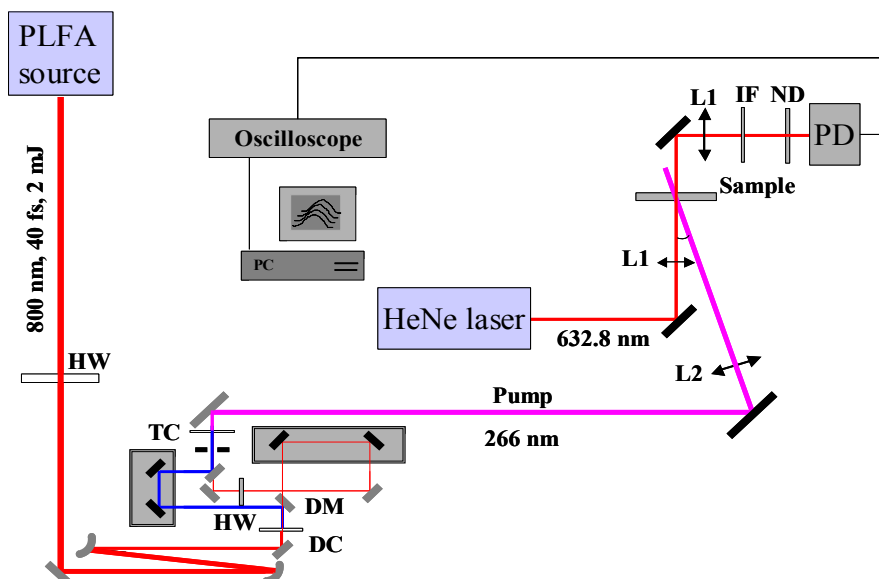


Figure S3: Experimental set-up for the nanosecond experiment in mesoporous media. HW: half waveplate, DC: doubling crystal, TC: tripling crystal, DM: dichroic mirror, L1: 0.15 m focusing lens, L2: 0.5 m focusing lens, IF: interferential filter centred at 632.8 nm with a 0.1 nm bandwidth, ND – neutral density, PD: photodiode (Thorlabs DET 210), oscilloscope (Tektronix TDS 784D). The pump energy was tuneable from 0 – 100 μ J.

The overlap between the pump and probe beams was verified using alumina foil. The beam diameter was measured using an Olympus BX41 microscope with an Olympus DP70 cooled digital colour camera system. The trace of the beam on the alumina foil was magnified, and its diameter measured (Figure S4).

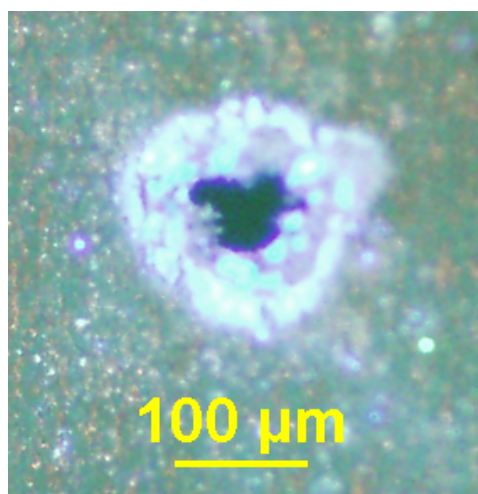


Figure S4: Trace of the pump beam in alumina foil

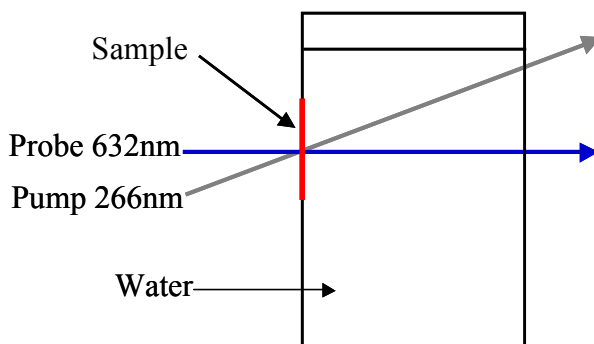


Figure S5: Schematic view of the sample cell.

In order to ensure the continuous hydration of the sample, a special cell was developed for their manipulation. It consisted of a UV-visible transparent cell, using on one of the sides the CPG sample as a window (supplementary material, figure S5). Experiments were performed on confined water and HClO₄ solutions (Sigma Aldrich chemicals). Ultrapure Millipore Milli-Q water, with the resistivity of 18.2 MΩ and less than 10 ppb organic carbon was used.

S.III. Calculation of the interaction length and of the concentration presented in figure 1 and 2.

S.III.1. Preparation of figure1

Assuming that the absorption of 2 UV photons in both water and solid matrix (SM) are simultaneously involved, the change of irradiance $I(z,r,t)$ (z , r , θ are the cylinder coordinates) along the optical path length z , considering that the nanostructuration scale to be small in front of the wavelength, is given by:

$$\frac{1}{I(z,r,t)} \frac{\partial I(z,r,t)}{\partial z} = -p \beta_{2H_2O} I(z,r,t) - (1-p) \beta_{2SM} I(z,r,t) \quad \text{Eq. 1}$$

where β_{2H_2O} , respectively β_{2SM} , is the two photon absorption (TPA) coefficient of water, respectively of the solid matrix, and p is the porosity of the sample in volume percentage.

For the numerical calculation we use the β_{2H_2O} and β_{2SM} coefficient values from Nikogosyan ³, and assume that the TPA coefficient for water is not altered by the confinement: $\beta_{2H_2O} = 4.9 \times 10^{-12} \text{ m} \cdot \text{W}^{-1}$; $\beta_{2SiO_2} = 2 \times 10^{-13} \text{ m} \cdot \text{W}^{-1}$ and $\beta_{2Al_2O_3} = 9.4 \times 10^{-13} \text{ m} \cdot \text{W}^{-1}$. Knowing the pump beam diameter ($FWHM = 100 \mu\text{m}$), the pulse duration (250 fs) and its energy ($70 \mu\text{J}$) we then deduce its irradiance to be $I_0 = 2 \text{ TW/cm}^2$.

Using these values, it is possible to numerically integrate Eq. 1 and, similarly to Pommeret et al⁴⁴, to compute the number of mol of photons absorbed per unit of volume as a function of the penetration depth. To convert the number of excited species to chemical species, the following two photon absorbed quantum yields: $\phi(HO^\bullet)=1$, $\phi(e_{aq}^-)=0.52$, $\phi(H_3O^+)=0.52$, $\phi(H^\bullet)=0.48$ were used in water.⁴ Owing to the very fast trapping of excited species in silica, we hypothesized $\phi(STE)=1$.⁵ The initial electron and exciton concentrations along the penetration depth are presented in figure 1. Most of the UV pump energy is absorbed within the first few tens of microns of the sample (figure 1) and considering that the CPG samples are 200 μm thick and the alumina 60 μm , the laser will hardly excite any water molecules from the solution in the cell. We must also notice that neither the CPG nor the bulk reservoir diffuse the visible probe beam.

S.III.2. Preparation of figure 2 and 3

From figure 1, we could define the interaction length ℓ_{90} as the position at which the pump intensity is divided by 10 i.e. 90% of the incident pulse energy has been absorbed. The calculated optical paths yields 56 μm for silica and 28 μm for alumina for $I_0 = 2 \text{ TW/cm}^2$.

Even though the initial concentration profile is very inhomogeneous, kinetic simulations presented in figure S6 show that secondary reactions induce a rapid levelling of the concentration along the penetration depth. In the probed time window ($> 1 \text{ ns}$), species' concentration along the pump light path are equivalent and the initial concentration peak near the entrance face has completely disappeared. Therefore, the optical densities measured on a $\text{ns}-\mu\text{s}$ time scale are not any more the average signal from a highly heterogeneous system, but are representative of the real solvated electron concentration in the pump beam optical path.

The time dependent optical transmittance of the sample was obtained by measuring the ratio $I(t)/I_0$, I_0 being the average light intensity before the pulse, and $I(t)$ the time dependent light intensity, both being measured by the photodiode PD in figure S6

Knowing the optical path and the time dependant optical transmittance, we could calculate the solvated electron concentrations using Beer Lambert law. The absorption coefficient ($\epsilon_{632}=20\times 10^3 \text{ M}^{-1}\text{cm}^{-1}$) used for this transformation was extracted from the work of Bartels and coll.⁶ The as obtained time dependant solvated electron concentrations are represented in figure 2.

S.IV. Kinetics simulation

S.IV.1 Chemistry in the pores at nanosecond time scale.

No simulation codes are capable to provide extensive kinetic simulation in heterogeneous media. Therefore, we had to rely on simulation in homogeneous media to test some kinetic hypothesis.

The following simulations were conducted using the Chemsimul Code⁷, based on the set of reactions and corresponding reaction rates listed hereafter. The reaction rates used are those generally agreed among the radiation chemistry community and are extracted from Buxton et al.⁸

RE1:	$OH^\bullet + OH^\bullet \rightarrow H_2O_2$	$k_1 = 5.5 \times 10^9$
RE2:	$OH^\bullet + e_{aq}^- \rightarrow OH^- + H_2O$	$k_2 = 3.0 \times 10^{10}$
RE3:	$OH^\bullet + H^\bullet \rightarrow H_2O$	$k_3 = 7 \times 10^9$
RE4:	$OH^\bullet + HO_2^\bullet \rightarrow O_2 + H_2O$	$k_4 = 7.5 \times 10^9$
RE5:	$OH^\bullet + O_2^{\bullet-} \rightarrow OH^- + O_2$	$k_5 = 8.8 \times 10^9$
RE6:	$OH^\bullet + H_2O_2 \rightarrow H_2O + HO_2^\bullet$	$k_6 = 2.7 \times 10^7$
RE7:	$OH^\bullet + H_2 \rightarrow H^\bullet + H_2O$	$k_7 = 4.7 \times 10^7$
RE8:	$e_{aq}^- + e_{aq}^- \rightarrow 2 * OH^- + H_2$	$k_8 = 5.5 \times 10^9$
RE9:	$e_{aq}^- + H^\bullet \rightarrow OH^- + H_2$	$k_9 = 2.5 \times 10^{10}$
RE10:	$e_{aq}^- + HO_2^\bullet \rightarrow H_2O_2 + OH^-$	$k_{10} = 1.3 \times 10^{10}$
RE11:	$e_{aq}^- + O_2^{\bullet-} \rightarrow HO_2^- + OH^-$	$k_{11} = 1.3 \times 10^{10}$
RE12:	$e_{aq}^- + H_2O_2 \rightarrow OH^- + OH^\bullet + H_2O$	$k_{12} = 1.1 \times 10^{10}$
RE13:	$e_{aq}^- + H^+ \rightarrow H^\bullet + H_2O$	$k_{13} = 2.3 \times 10^{10}$
RE14:	$e_{aq}^- + H_2O \rightarrow H^\bullet + OH^- + H_2O$	$k_{14} = 1.0 \times 10^3$
RE15:	$e_{aq}^- + O_2 \rightarrow O_2^{\bullet-} + H_2O$	$k_{15} = 1.9 \times 10^{10}$
RE16:	$H^\bullet + H^\bullet \rightarrow H_2$	$k_{16} = 6.0 \times 10^9$
RE17:	$H^\bullet + HO_2^\bullet \rightarrow H_2O_2$	$k_{17} = 2.0 \times 10^{10}$
RE18:	$H^\bullet + O_2^{\bullet-} \rightarrow HO_2^-$	$k_{18} = 2.0 \times 10^{10}$

RE19:	$H^\bullet + H_2O_2 \rightarrow OH^\bullet + H_2O$	$k_{19} = 9.0 \times 10^7$
RE20:	$H^\bullet + OH^- \rightarrow e_{aq}^-$	$k_{20} = 2.2 \times 10^7$
RE21:	$H^\bullet + O_2 \rightarrow HO_2^\bullet$	$k_{21} = 1.2 \times 10^{10}$
RE22:	$HO_2^\bullet + HO_2^\bullet \rightarrow O_2 + H_2O_2$	$k_{22} = 8.3 \times 10^5$
RE23:	$HO_2^\bullet + O_2^\bullet \rightarrow O_2 + HO_2^-$	$k_{23} = 9.7 \times 10^7$
RE24:	$O_2^\bullet + O_2^\bullet \rightarrow O_2 + O_2^{--}$	$k_{24} = 5.0 \times 10^3$
RE25:	$HO_2^\bullet \rightarrow O_2^- + H^+$	$k_{25} = 8.0 \times 10^5$
RE26:	$O_2^- + H^+ \rightarrow HO_2$	$k_{26} = 5.0 \times 10^{10}$
RE27:	$H_2O_2 + OH^- \rightarrow HO_2^- + H_2O$	$k_{27} = 5.0 \times 10^8$
RE28:	$HO_2^- + H_2O \rightarrow H_2O_2 + OH^-$	$k_{28} = 5.73 \times 10^4$
RE29:	$H_2O_2 \rightarrow H_2O + O$	$k_{29} = 2.0 \times 10^{-5}$
RE30:	$O^\bullet + O^\bullet \rightarrow O_2$	$k_{30} = 1.0 \times 10^{10}$
RE31:	$O_2^{--} + H_2O \rightarrow HO_2^- + OH^-$	$k_{31} = 5.0 \times 10^5$
RE32:	$H^+ + OH^- \rightarrow H_2O$	$k_{32} = 1.43 \times 10^{11}$
RE33:	$H_2O \rightarrow H^+ + OH^-$	$k_{33} = 2.599 \times 10^{-5}$

The initial concentrations of the radical species (e_{aq}^-), HO^\bullet , and H^\bullet were taken from Figure 1,

The calculated evolution of the aqueous electron concentration along the penetration depth at different time delays is presented in figure S6.

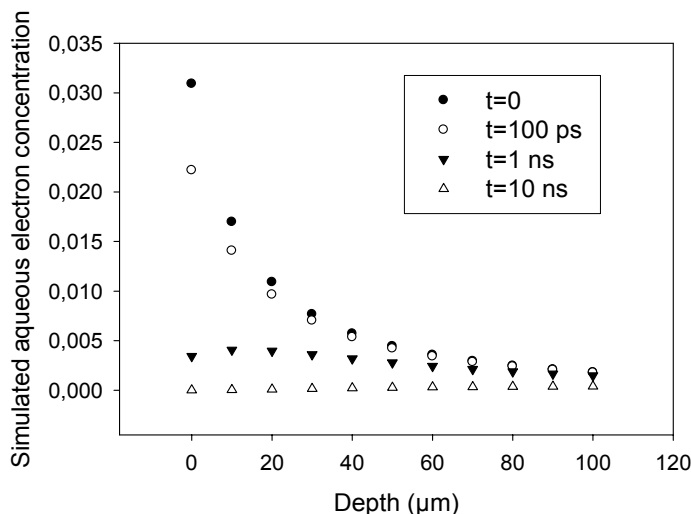


Figure S6: Calculated evolution of the concentration profile of hydrated electron as a function of the sample depth and the time assuming that the solid matrix does not play any role in the confined water chemistry.

S.IV.2 Origin of the delayed production.

In order to test the chemical effect of electron injection from a silica reservoir, an additional reaction was inserted in the upper described scheme, with a reaction rate constant that was systematically varied from 10^6 to 10^9 s^{-1} . The initial exciton concentration used for the calculations (SE) was taken from the deposition profile shown in Figure 1.



The evolution of the aqueous electron concentration is presented in figure S7 for various values of k_{34} . An injection occurring too early ($k_{34} = 1 \times 10^9 \text{ s}^{-1}$) would result in a non-observable delayed production: the injected electrons would rapidly react with the reactive species already present in solution. A secondary electron production is observed for delayed injections: $k_{34} < 1 \times 10^8 \text{ s}^{-1}$. Indeed, the delayed electron production observed 30 ns after the pulse in CPG 50 nm (inset of figure S7) can be reproduced by an electron injection occurring with a typical 10^7 s^{-1} time constant.

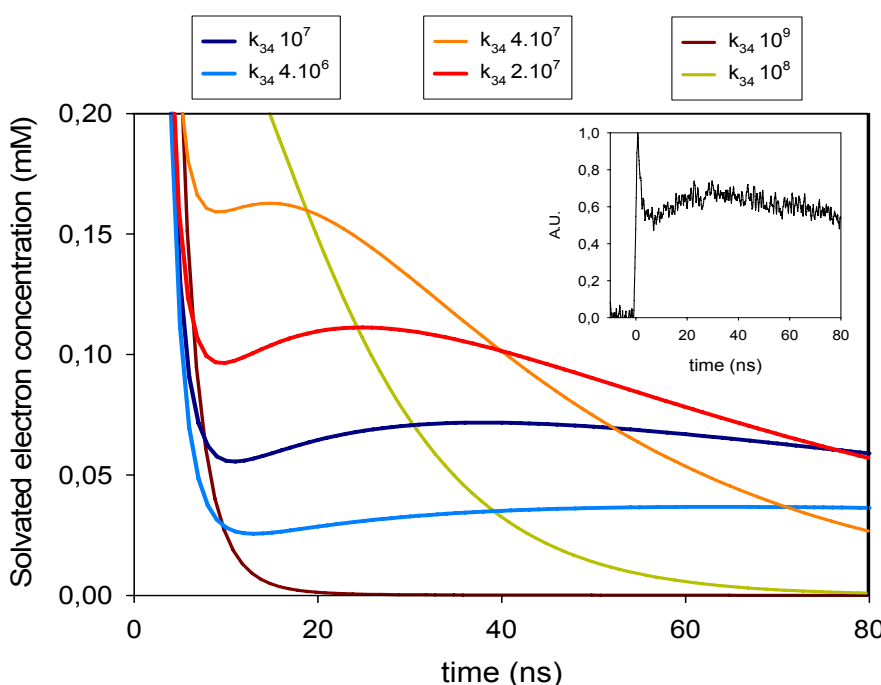


Figure S7: Influence of the self trapped exciton dissociation kinetic constant at the solid water interface on the fate of the hydrated electron in confined media.

In order to test if silica excitons can be the source of this injection, we performed a crude evaluation of the time they required to reach the silica water interface. In the CPG 50 nm sample, the distance a tracer can go in direct line before reaching an interface (i.e. the mean chord length see table S1) can be evaluated to be 10 nm from the specific volume over specific surface ratio.⁹ In CPG 1 nm, the same length is only of 0.9 nm .

An exciton diffusion constant D can be extrapolated from the data gathered by Costantini et al.¹⁰ At 85 K, they measured a diffusion coefficient of $D = 5 \times 10^{-10} \text{ cm}^2 \cdot \text{s}^{-1}$ and activation energy of 0.1 eV. Therefore, at 300 K, the diffusion coefficient should be $D = 1 \times 10^{-5} \text{ cm}^2 \cdot \text{s}^{-1}$. Thus we estimated that the typical time needed for an STE to reach the solid/water interface in CPG 50 nm is of the order of 100 ns. Therefore, the characteristic reaction rate $k_{34} = 1 \times 10^7 \text{ s}^{-1}$ associated to the electron secondary production in this glass is compatible to an exciton diffusion from the interior of the porous material to the surface.

In CPG 1nm, STE, provided they can form, would reach the solid/water interface in less than a nanosecond. Therefore, any secondary electron production that may occur in small pore glasses can not be observed in the time window we probed.

REFERENCES

- ¹ W. Haller, *Nature*, 1965, **206**, 693-696.
- ² D. Enke, F. Janowski and W. Schwieger, *Micro. Meso. Mater.*, 2003, **60**, 19-30.
- ³ A. Dragonmir, J. G. McInerney and D. N. Nikogosyan, *Appl. Optics*, 2002, **41**, 4365-4376.
- ⁴ S. Pommeret, F. Gobert, M. Mostafavi, I. Lampre and J. C. Mialocq, *J. Phys. Chem. A*, 2001, **105**, 11400-11406.
- ⁵ P. Audebert, P. Daguzan, A. D. Santos, J. C. Gauthier, J. P. Geindre, S. Guizard, G. Hamoniaux, K. Krastev, P. Martin, G. Petite and A. Antonietti, *Phys. Rev. Lett.*, 1994, **73**, 1990.
- ⁶ P. M. Hare, E. A. Price, and D. M. Bartels, *J. Phys. Chem. A*, 2008, **112**, 6800–6802
- ⁷ P. Kirkegaard, E. Bjergbakke and J. V. Olsen, CHEMSIMUL: A chemical kinetics software package, 2007.
- ⁸ G. V. Buxton, C. L. Greenstock, W. P. Helman and A. B. Ross, *J. Phys. Chem. Ref. Data*, 1988, **17**, 513-531.
- ⁹ B. Smarsly, C. Göltner, M. Antonietti, W. Ruland and E. Hoinkis, *J. Phys. Chem. B*, 2001, **105**, 831-840.
- ¹⁰ J. M. Costantini, F. Brisard, G. Biotteau, E. Balanzat and B. Gervais, *J. Appl. Phys.*, 2000, **88**, 1339-1345.